EFFECT OF THE BOUNDARY CONDITIONS ON THE DYNAMIC BEHAVIOURS OF SUBSEA FREE-SPANNING PIPELINES

(DOI No: 10.3940/rina.ijme.2018.a2.467)

T T Li, **C An*** and **M L Duan**, Institute for Ocean Engineering, China University of Petroleum – Beijing, China, **H Huang**, Petroleum Exploration and Production Research Institute, Sinopec, China, and **W Liang**, College of Mechanical and Transportation Engineering, China University of Petroleum – Beijing, China

SUMMARY

This paper establishes a fast and accurate solution of the dynamic behaviours of subsea free-spanning pipelines under four different boundary conditions, based on GITT - the generalised integral transform technique. The fluid-structure interaction model is proposed by combining a linear structural equation and a non-linear distributed wake oscillator model, which simulates the effect of external current acting on the pipeline. The eigenvalue problems for the cross-flow vibration of the free-spanning submarine pipeline conveying internal fluid for four different boundary conditions are examined. The solution method of the natural frequency based on GITT is proposed. The explicit analytical formulae for the cross-flow displacement of the pipeline free span are derived, and the mode shapes and dynamic behaviours of the pipeline free span are discussed with different boundary conditions. The methodology and results in this paper can also expand to solving even more complicated boundary-value problems.

1. INTRODUCTION

Due to seabed unevenness, pipeline crossings, tie-in to subsea structures, sleepers, soil scouring, sand waves, etc., it is inevitable that the free span of subsea pipelines develops in offshore/underwater projects. When a free span forms, the structural behaviours of the free spanning part will be different from the shoulder parts which rest on the seabed (Ronold, 1995). Under the backdrop that the oil supplies onshore and even in shallow waters which are easily accessible are declining, the exploration of oil and gas is now targeting at deeper waters (Bouchonneau et al, 2010; Fyrileiv et al, 2013 and Sollund et al, 2015). The existence of subsea free-spanning pipelines brings rigorous challenges for offshore/underwater engineering. Sollund et al. (2015) summarised the three major categories of risks that the free span poses to pipeline integrity, i.e. extensive bending/local buckling due to static weight, free spans being hooked by anchors or trawling equipment, and vortex-induced vibrations (VIV).

Vortex-induced vibrations (VIV) is defined as motions triggered on bluff bodies by interaction with an external flow. It determines, to a large extent, the dynamic characteristics of the subsea free-spanning pipeline, and the boundary conditions is one of the factors that affect the VIV behaviours of the free span. DNV-RP-F105 (2006) suggested that the free-spanning pipeline can be simplified as a beam model with pinned-pinned or fixed-fixed ends for VIV analysis. And there are a large number of theoretical, numerical and experimental studies that follow the above mentioned principle. For instance, Lou et al. (2005) conducted a finite element analysis of pinned-pinned subsea free-spanning pipelines; Kaewunrue et al. (2005) studied the nonlinear free vibration of marine pipes to determine the natural frequencies and mode shapes based on a pinned-pinned pipe model; Brushi and Vital (1991) carried out an experiment for the VIV behaviours of pipes with pinned-pinned, and clamped-clamped boundary conditions; Gu et al. (Gu et al, 2013a and Gu et al, 2013b) studied the VIV of a pinned-pinned flexible cylinder by carrying out a towing tank experiment and adopted an integral transform technique to solve the dynamic characteristics of a clamped-clamped pipe.

Due to the complexity of the harsh marine environment and the vibration behaviour of the pipeline system per se, proposing the appropriate boundary value problems to describe the boundary conditions for subsea free-spanning pipelines is not easy, not to mention solving the eigenvalue problems of structures with complicated boundary conditions. That said, attempts are done by researchers to study more complicated boundary condition problems. Choi (2001) proposed a calculation formula for the maximum allowable span length under fixed-fixed, pinned-pinned, fixed-pinned and fixed-free boundary conditions. Meng et al. (2017) studied the cross-flow vibration of a fixed-free pipe discharging fluid, and Cui and Tani (2008) studied the stability of a fixed-free pipe discharging and aspirating fluid. To make the boundary condition of the subsea free-spanning pipeline more close to the reality, Ai et al. (2009) proposed a spring-supported model to simulate the pipe-soil interaction at the span shoulders, while the two ends of the free-spanning pipeline system remain simple-supported.

However, free-spanning pipeline analyses typically involve a significant amount of parametric studies due to variations in span lengths, axial forces, flow and current velocities, boundary conditions, etc. (Tang et al, 2015, and Yang et al, 2017). Methods such as numerical simulation or large-scale experiments are quite time-consuming. It is highly desirable to establish a method based on analytical approaches, which can radically reduce the calculation time. The present paper is aimed at exploring a fast and accurate method for solving complicated boundary value problems. Firstly, a fluid-structure interaction model which combines a linear structural equation and non-linear distributed wake oscillator model simulating the effect of external current

acting on the free-spanning pipeline is proposed, and the eigenvalue problems of the cross-flow vibration of the free-spanning pipeline under four different boundary conditions are solved. Secondly, the governing equation system is solved by GITT - the generalised integral transform technique, and the explicit analytical formulae for the cross-flow displacement of the pipeline free span are derived. Thirdly, the natural frequency of the free span system is solved based on GITT, which is validated against the theoretical results. In addition, the mode shapes and the dynamic behaviours are discussed.

2. PROBLEM DEFINITION

2.1 MODEL DESCRIPTION

Consider an elastic free-spanning submarine pipeline conveying internal fluid as shown in Figure 1. A Cartesian coordinate with its origin at the left end of the free span is set up, where the *x*-axis is the initial axis of a static pipeline, the *y*-axis is parallel to the direction of the current flow, and the *z*-axis is in the direction opposing gravity, along which the free-spanning pipeline vibrates. The Bernoulli-Euler beam equation is adopted to describe the transverse vibration of the pipeline. The governing equation system of the cross-flow vibration of the free-spanning submarine pipeline is given as (Lou et al, 2005 and Li et al, 2016):

$$\begin{cases} EI\dfrac{\partial^4 z}{\partial x^4}+(m_i U^2+PA_i-T_a)\dfrac{\partial^2 z}{\partial x^2}+2m_i U\dfrac{\partial^2 z}{\partial x\partial t}+ \\ (r_s+r_f)\dfrac{\partial z}{\partial t}+m\dfrac{\partial^2 z}{\partial t^2}=\dfrac{\rho_e V^2 DC_{L0}}{4}q \\ \dfrac{\partial^2 q}{\partial t^2}+\varepsilon\Omega_f(q^2-1)\dfrac{\partial q}{\partial t}+\Omega_f{}^2 q=\dfrac{\alpha}{D}\dfrac{\partial^2 z}{\partial t^2} \end{cases} \quad (1)$$

The pipeline is assumed to be cylindrical with both constant outer and inner diameters, respectively symbolised as D and D_i; its inner cross section area is symbolised as A_i; the free-spanning pipeline is subject to steady internal flow, with a constant velocity of U, and to uniform current, with a constant velocity of V; the axial tension is T_a; the internal pressure is P; the spanlength is L. m_p, m_i and m_e is the mass per unit length of the pipeline, the internal fluid and the added mass due to external fluid, and m is the summation of the three; m_e can be calculated by $m_e=\dfrac{C_M\pi\rho_e D^2}{4}$, where C_M is the added mass coefficient, and ρ_e is the density of the external fluid; EI is the flexural stiffness; St is the Strouhal number; r_s is the structural damping; r_f is the fluid added damping, equalling to $\gamma\,\Omega_f\rho_e D^2$, where γ is a coefficient related to the mean sectional drag coefficient of the pipe - C_D, expressed as $C_D/(4\pi St)$; the term on the right side of the first equation $\dfrac{\rho_e V^2 DC_{L0}}{4}q$ denotes the lift force exerted on the pipeline by the current; $q=2C_L(x,t)/C_{L0}$ is the reduced fluctuating lift coefficient, where C_{L0} is the reference lift coefficient that can be obtained through the observation of a fixed structure subject to vortex shedding, and C_L is the lift coefficient.

The second equation in the governing equation system Equation 1 is a wake oscillator model (Facchinetti et al, 2004). It is to simulate the fluid force acting on the free span. $\Omega_f=2\pi StU/D$ denotes the vortex-shedding frequency; $\dfrac{\alpha}{D}\dfrac{\partial^2 z}{\partial t^2}$ describes the effect of the pipe motion on the near wake. It can be seen that the coupling is through acceleration. The values of the van der Pol parameter ε and scaling parameter α can be derived from the experimental results from Facchinetti et al. (2004). Under the acceleration coupling model the value of ε is 0.3, and α 12. The values of other fluid parameters in the mathematical model are as follows: C_D = 1.2, C_M = 1, St = 0.2.

By introducing the following dimensionless variables:

$$x^*=\frac{x}{L},\ z^*=\frac{z}{D},\ t^*=\frac{t}{L^2}\sqrt{\frac{EI}{m_p}},\ U^*=UL\sqrt{\frac{m_p}{EI}},\quad (2)$$
$$V^*=VL\sqrt{\frac{m_p}{EI}},\ \Omega_f{}^*=\Omega_f L^2\sqrt{\frac{m_p}{EI}},\ \beta=\frac{\rho_e U^{*2}C_{L0}L^2}{4m_p}$$

the governing equation system Equation 1 is then turned to (omitting the asterisks for simplicity):

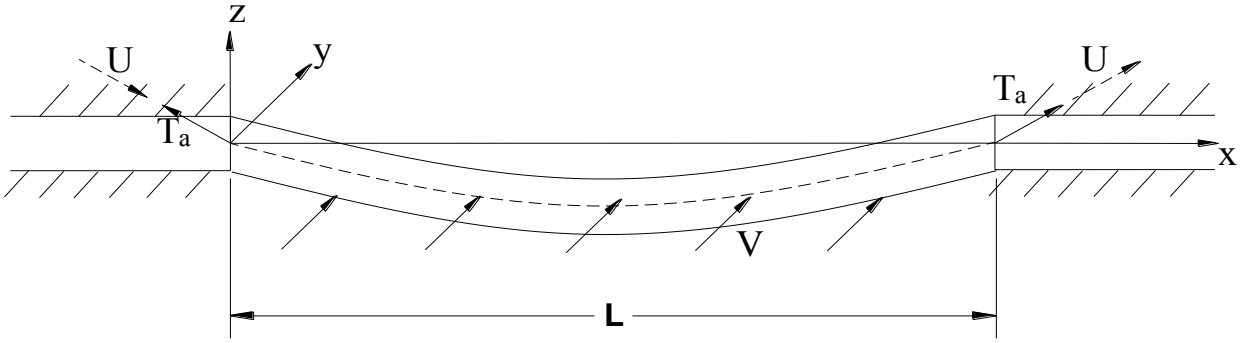

Figure 1: Schematic diagram of a fluid-conveying free-spanning submarine pipeline.

$$\begin{cases} \dfrac{\partial^4 z}{\partial x^4}+(\dfrac{m_i U^2}{m_p}+\dfrac{PA_i L^2}{EI}-\dfrac{T_a L^2}{EI})\dfrac{\partial^2 z}{\partial x^2}+\dfrac{2m_i U}{m_p}\dfrac{\partial^2 z}{\partial x \partial t}+ \\ (r_s+r_f)\dfrac{L^2}{\sqrt{m_p EI}}\dfrac{\partial z}{\partial t}+\dfrac{m}{m_p}\dfrac{\partial^2 z}{\partial t^2}=\beta q \\ \dfrac{\partial^2 q}{\partial t^2}+\varepsilon\Omega_f(q^2-1)\dfrac{\partial q}{\partial t}+\Omega_f{}^2 q=\alpha\dfrac{\partial^2 z}{\partial t^2} \end{cases} \tag{3}$$

2.2 EIGENVALUE PROBLEMS

The eigenvalue problems of the transverse displacement of the free span and the wake variable can be written respectively as:

$$\frac{\mathrm{d}^4 X_i(x)}{\mathrm{d}x^4}=\phi_i{}^4 X_i(x),\ 0<x<1 \tag{4a}$$

$$\frac{\mathrm{d}^4 Y_k(x)}{\mathrm{d}x^4}=\varphi_k{}^4 Y_k(x),\ 0<x<1 \tag{4b}$$

where X_i and ϕ_i are the eigenfunction and the eigenvalue of problem Equation 4a; likewise Y_k and φ_k are the eigenfunction and the eigenvalue of problem Equation 4b. The eigenfunctions both satisfy the following orthogonality,

$$\int_0^1 X_i(x)X_j(x)\mathrm{d}x=\delta_{ij}N_i \tag{5a}$$

$$\int_0^1 Y_k(x)Y_l(x)\mathrm{d}x=\delta_{kl}N_k \tag{5b}$$

where δ_{ij} and δ_{kl} is the Kronecker delta. For $i\neq j$, $\delta_{ij}=0$; and for $i\neq j$, $\delta_{ij}=1$. Likewise, for $k\neq l$, $\delta_{kl}=0$; for $k=l$, $\delta_{kl}=1$.

The normalised integrals are

$$N_i=\int_0^1 X_i{}^2(x)\mathrm{d}x \tag{6a}$$

$$N_k=\int_0^1 Y_k{}^2(x)\mathrm{d}x \tag{6b}$$

Hence, the general solution for the eigenfunctions are given by

$$X_i(x)=C_1\cos\phi_i x+C_2\sin\phi_i x+C_3\cosh\phi_i x+C_4\sinh\phi_i x \tag{7a}$$

$$Y_k(x)=D_1\cos\varphi_k x+D_2\sin\varphi_k x+D_3\cosh\varphi_k x+D_4\sinh\varphi_k x \tag{7b}$$

The unknowns (C_1, C_2, C_3, C_4, ϕ and C_1, C_2, C_3, C_4, φ) are determined by the boundary conditions. The four different boundary conditions discussed in the present paper are expressed as:

- fixed-fixed boundary condition:

$$X_i(0)=0,\ \frac{\mathrm{d}X_i(0)}{\mathrm{d}x}=0,\ X_i(1)=0,\ \frac{\mathrm{d}X_i(1)}{\mathrm{d}x}=0 \tag{8a}$$

$$Y_k(0)=0,\ \frac{\mathrm{d}Y_k(0)}{\mathrm{d}x}=0,\ Y_k(1)=0,\ \frac{\mathrm{d}Y_k(1)}{\mathrm{d}x}=0 \tag{8b}$$

- fixed-pinned boundary condition:

$$X_i(0)=0,\ \frac{\mathrm{d}X_i(0)}{\mathrm{d}x}=0,\ X_i(1)=0,\ \frac{\mathrm{d}^2X_i(1)}{\mathrm{d}x^2}=0 \tag{9a}$$

$$Y_k(0)=0,\ \frac{\mathrm{d}Y_k(0)}{\mathrm{d}x}=0,\ Y_k(1)=0,\ \frac{\mathrm{d}^2Y_k(1)}{\mathrm{d}x^2}=0 \tag{9b}$$

- fixed-free boundary condition:

$$X_i(0)=0,\ \frac{\mathrm{d}X_i(0)}{\mathrm{d}x}=0,\ \frac{\mathrm{d}^2X_i(1)}{\mathrm{d}x^2}=0,\ \frac{\mathrm{d}^3X_i(1)}{\mathrm{d}x^3}=0 \tag{10a}$$

$$Y_k(0)=0,\ \frac{\mathrm{d}Y_k(0)}{\mathrm{d}x}=0,\ \frac{\mathrm{d}^2Y_k(1)}{\mathrm{d}x^2}=0,\ \frac{\mathrm{d}^3Y_k(1)}{\mathrm{d}x^3}=0 \tag{10b}$$

- pinned-pinned boundary condition:

$$X_i(0)=0,\ \frac{\mathrm{d}^2X_i(0)}{\mathrm{d}x^2}=0,\ X_i(1)=0,\ \frac{\mathrm{d}^2X_i(1)}{\mathrm{d}x^2}=0 \tag{11a}$$

$$Y_k(0)=0,\ \frac{\mathrm{d}^2Y_k(0)}{\mathrm{d}x^2}=0,\ Y_k(1)=0,\ \frac{\mathrm{d}^2Y_k(1)}{\mathrm{d}x^2}=0 \tag{11b}$$

The eigenvalue problems (4a) and (4b) are now solved for four different conditions:

- fixed-fixed boundary condition:

$$X_i(x)=\sin\phi_i x-\sinh\phi_i x+\frac{(\sinh\phi_i-\sin\phi_i)(\cosh\phi_i x-\cos\phi_i x)}{\cosh\phi_i-\cos\phi_i} \tag{12a}$$

$$Y_k(x)=\sin\varphi_k x-\sinh\varphi_k x+\frac{(\sinh\varphi_k-\sin\varphi_k)(\cosh\varphi_k x-\cos\varphi_k x)}{\cosh\varphi_k-\cos\varphi_k} \tag{12b}$$

where

$$\cosh\phi_i\cos\phi_i=1\ (i=1,\ 2,\ 3,\ \ldots) \tag{13a}$$

and

$$\cosh\varphi_k\cos\varphi_k=1\ (k=1,\ 2,\ 3,\ \ldots) \tag{13b}$$

- fixed-pinned boundary condition:

$$X_i(x)=\sin\phi_i x-\sinh\phi_i x+\frac{(\sinh\phi_i-\sin\phi_i)(\cosh\phi_i x-\cos\phi_i x)}{\cosh\phi_i-\cos\phi_i} \tag{14a}$$

$$Y_k(x)=\sin\varphi_k x-\sinh\varphi_k x+\frac{(\sinh\varphi_k-\sin\varphi_k)(\cosh\varphi_k x-\cos\varphi_k x)}{\cosh\varphi_k-\cos\varphi_k} \tag{14b}$$

where

$$\tanh\phi_i\tan\phi_i=1\ (i=1,\ 2,\ 3,\ \ldots) \tag{15a}$$

and

$$\tanh\varphi_k\tan\varphi_k=1\ (k=1,\ 2,\ 3,\ \ldots) \tag{15b}$$

- fixed-free boundary condition:

$$X_i(x)=\sin\phi_i x-\sinh\phi_i x+\frac{(\sinh\phi_i+\sin\phi_i)(\cosh\phi_i x-\cos\phi_i x)}{\cosh\phi_i+\cos\phi_i} \tag{16a}$$

$$Y_k(x)=\sin\varphi_k x-\sinh\varphi_k x+\frac{(\sinh\varphi_k+\sin\varphi_k)(\cosh\varphi_k x-\cos\varphi_k x)}{\cosh\varphi_k+\cos\varphi_k} \tag{16b}$$

where

$$\cosh\phi_i\cos\phi_i=-1\ (i=1,\ 2,\ 3,\ \ldots) \tag{17a}$$

and

$$\cosh\varphi_k\cos\varphi_k=-1\ (k=1,\ 2,\ 3,\ \ldots) \tag{17b}$$

- pinned-pinned boundary condition:

$$X_i(x)=\sin(\phi_i x) \tag{18a}$$

$$Y_k(x)=\sin(\varphi_k x) \tag{18b}$$

where

$$\phi_i=i\pi\ (i=1,\ 2,\ 3,\ \ldots) \tag{19a}$$

and

$$\varphi_k=i\pi\ (k=1,\ 2,\ 3,\ \ldots) \tag{19b}$$

3. INTEGRAL TRANSFORM SOLUTION

When the eigenvalue problems are solved, one can proceed with using GITT to solve the governing equation system Equation 3. Following the principle of GITT, the integral transform pair - the integral transform itself and the inversion formula is put forward.

For the transverse displacement of the free span:

$$\bar{z}_i(t)=\int_0^1\tilde{X}_i(x)z(x,t)\,\mathrm{d}x\ ,\ \text{transform} \tag{20a}$$

$$z(x,t)=\sum_{i=1}^{\infty}\tilde{X}_i(x)\bar{z}_i(t)\ ,\ \text{inversion} \tag{20b}$$

For the wake variable:

$$\bar{q}_k(t)=\int_0^1\tilde{Y}_k(x)q(x,t)\,\mathrm{d}x\ ,\ \text{transform} \tag{21a}$$

$$q(x,t)=\sum_{k=1}^{\infty}\tilde{Y}_k(x)\bar{q}_k(t)\ ,\ \text{inversion} \tag{21b}$$

where $\tilde{X}_i(x)=\dfrac{X_i(x)}{N_i^{1/2}}$ and $\tilde{Y}_k(x)=\dfrac{Y_k(x)}{N_i^{1/2}}$ are the normalised eigenfunctions.

The next step is to use GITT to transform the governing equation system in order that it is in the appropriate form that the results can be calculated. Multiplied by operators $\int_0^1\tilde{X}_i(x)\,\mathrm{d}x$ and $\int_0^1\tilde{Y}_k(x)\,\mathrm{d}x$ respectively, the partial differential equation system (3) is transferred to the following set of ordinary differential equation system, where the spatial coordinate x is eliminated:

$$\begin{cases}\phi_1^4\bar{z}_i(t)+(\dfrac{m_1U^2}{m_p}+\dfrac{PA_1L^2}{EI}-\dfrac{T_aL^2}{EI})\sum_{j=1}^{\infty}A_{ij}\bar{z}_j(t)+\dfrac{2m_1U}{m_p}\sum_{j=1}^{\infty}B_{ij}\dfrac{\mathrm{d}\bar{z}_j(t)}{\mathrm{d}t}+\\ (r_s+r_f)\dfrac{L^2}{\sqrt{EIm_p}}\dfrac{\mathrm{d}\bar{z}_i(t)}{\mathrm{d}t}+\dfrac{m}{m_p}\dfrac{\mathrm{d}^2\bar{z}_i(t)}{\mathrm{d}t^2}=\beta\sum_{k=1}^{\infty}C_{ik}\bar{q}_k(t)\\ \dfrac{\mathrm{d}^2\bar{q}_k(t)}{\mathrm{d}t^2}+\varepsilon\Omega_f\sum_{l=1}^{\infty}\sum_{r=1}^{\infty}\sum_{s=1}^{\infty}D_{klrs}\bar{q}_l(t)\bar{q}_r(t)\dfrac{\mathrm{d}\bar{q}_s(t)}{\mathrm{d}t}-\\ \varepsilon\Omega_f\dfrac{\mathrm{d}\bar{q}_k(t)}{\mathrm{d}t}+\Omega_f{}^2\bar{q}_k(t)=\alpha\sum_{i=1}^{\infty}E_{ki}\dfrac{\mathrm{d}^2\bar{z}_i(t)}{\mathrm{d}t^2}\end{cases} \tag{22a}$$

where the coefficients are determined by the following integrals:

$$\begin{aligned}&A_{ij}=\int_0^1\tilde{X}_i(x)\frac{\mathrm{d}^2\tilde{X}_j(x)}{\mathrm{d}x^2}\mathrm{d}x,\ B_{ij}=\int_0^1\tilde{X}_i(x)\frac{\mathrm{d}\tilde{X}_j(x)}{\mathrm{d}x}\mathrm{d}x,\\ &C_{ik}=\int_0^1\tilde{X}_i(x)\tilde{Y}_k(x)\mathrm{d}x,\ D_{klrs}=\int_0^1\tilde{Y}_k(x)\tilde{Y}_l(x)\tilde{Y}_r(x)\tilde{Y}_s(x)\mathrm{d}x,\\ &E_{ki}=\int_0^1\tilde{Y}_k(x)\tilde{X}_i(x)\mathrm{d}x\end{aligned} \tag{22b}$$

For calculation, the expansions for $z(x,t)$ and $q(x,t)$ are truncated to N orders. When $\bar{z}_i(t)$ and $\bar{q}_k(t)$ are numerically evaluated with N orders, the inversion formulas Equations 20b and 21b are than applied to obtain the semi-analytical expressions for the non-dimensional $z(x,t)$ and $q(x,t)$.

4. RESULTS AND DISCUSSION

4.1 NATURAL FREQUENCIES BY GITT

The main parameters for the pipeline free span and the fluid are shown in Table 1. The internal flow velocity is set as zero. And for the initial conditions, a random noise with an amplitude of order $O(10^{-3})$ is applied to $z(x,0)$:

$$z(x,0)=O(10^{-3}),\ \frac{\partial z(x,0)}{\partial t}=0,\ q(x,0)=0,\ \frac{\partial q(x,0)}{\partial t}=0 \tag{23}$$

Table 1 Geometric and physical properties of submarine pipeline, internal flow and external current.

Symbol	Value	Unit
Submarine pipeline		
L	40	m
D	0.35	m
D_i	0.325	m
ρ_p	8200	kg/m^3
ξ	0.005	
E	2.0×10^{11}	Pa
Internal fluid		
ρ_i	908.2	kg/m^3
External fluid		
ρ_e	1025	kg/m^3
C_D	1.2	
C_M	1	
C_{L0}	0.3	
α	12	
ε	0.3	
St	0.2	

Table 2 Fundamental natural frequency of the pipeline free span under different boundary conditions

Boundary condition	Results by GITT	Fundamental natural frequency $f_{s,1}$ (Hz)
Fixed-fixed	2.20	0.81
Fixed-pinned	1.53	0.56
Fixed-free	0.35	0.13
Pinned-pinned	0.98	0.36

Figure 2 presents the free vibration time history and frequency analysis of the free span midpoint for four different boundary conditions. The spectrogram for each boundary condition is obtained by the Fast Fourier Transform of the time histories. Since the governing equation system is non-dimensional, results calculated by GITT is also non-dimensional. The dominant frequency in the spectrogram for each boundary condition is the fundamental natural frequency of the free span. By conversion, the fundamental structural natural frequency in Hz is summarised in Table 2.

In order to validate the correctness of GITT solutions, the results in Table 2 is verified against the theoretical result, calculated by Equation 24.

$$f_s=\frac{\phi_i^2}{2\pi L^2}\sqrt{\frac{EI}{(m_p+m_i+m_e)}} \tag{24}$$

The first solution of the eigenvalue ϕ_1, obtained through Equations 13a, 15a, 17a, 19a, respectively are 4.730041, 3.926602, 1.875104, π。 And by introducing the values of ϕ_1 to Equation 24, the corresponding natural frequency of the free spanning pipeline conveying internal flow with zero velocity are 0.81 Hz, 0.56 Hz, 0.13 Hz, 0.36 Hz, respectively for boundary conditions of the fixed-fixed, the fixed-pinned, the fixed-free and the pinned-pinned. By comparison, the results calculated by GITT is consistent with the theoretical results. This also proves the validity of the GITT solution.

4.2 MODE SHAPE ANALYSIS

When the structural natural frequency is determined, the structural damping can then be evaluated by relating to the natural frequency with $r_s=4\pi m f_s\xi$, where ξ is the damping ratio, the value of which, in this case, is taken as 0.005. Figure 3 depicts the mode shapes of the pipeline free span under different boundary conditions, at U = 0.5 and Vr = 6, where Vr is a normalised current velocity (reduced velocity) calculated by $Vr=V/Df_s$.

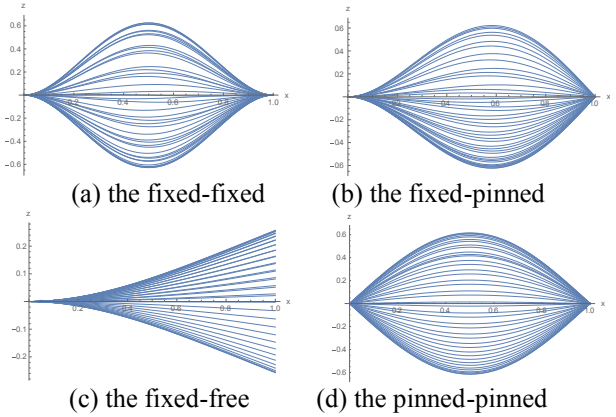

(a) the fixed-fixed (b) the fixed-pinned

(c) the fixed-free (d) the pinned-pinned

Figure 3: Mode shapes of the free span under different boundary conditions

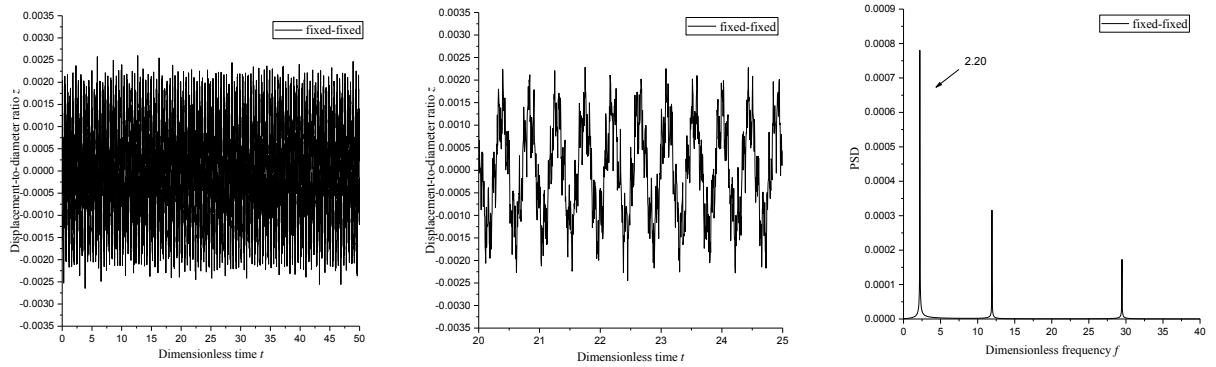

(a) fixed-fixed boundary condition

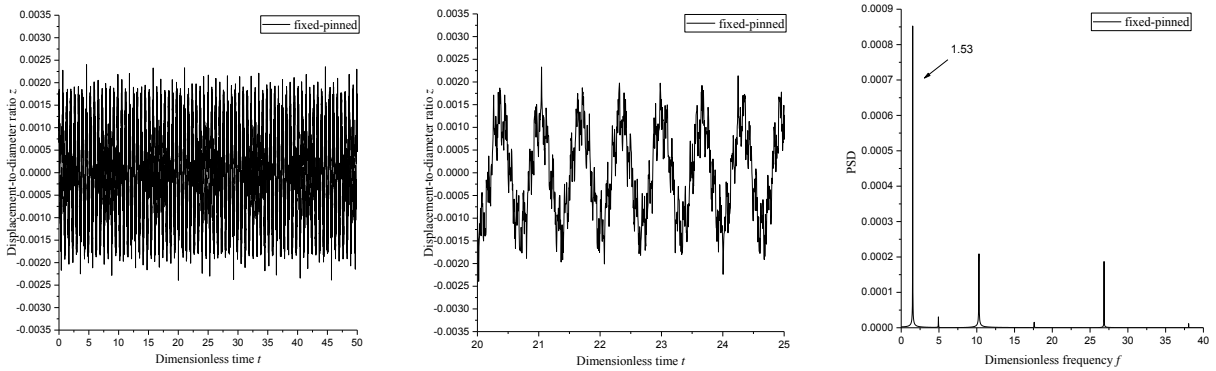

(b) fixed-pinned boundary condition

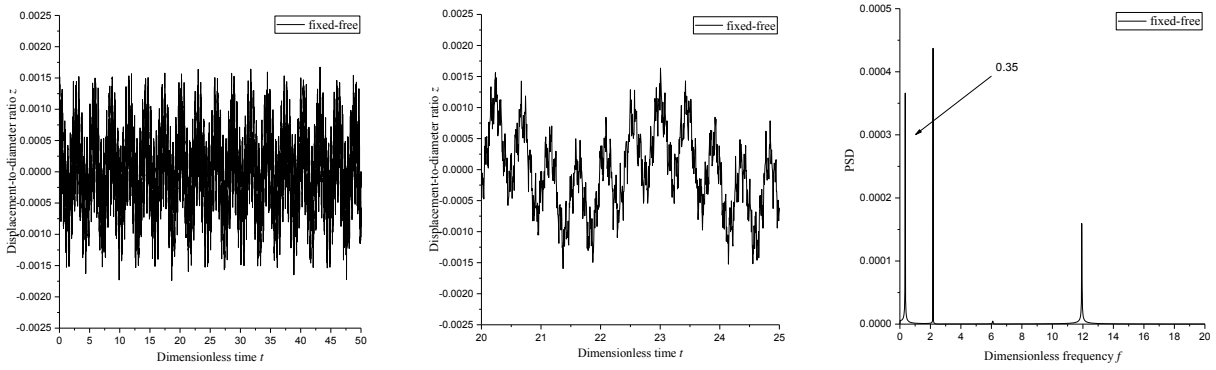

(c) fixed-free boundary condition

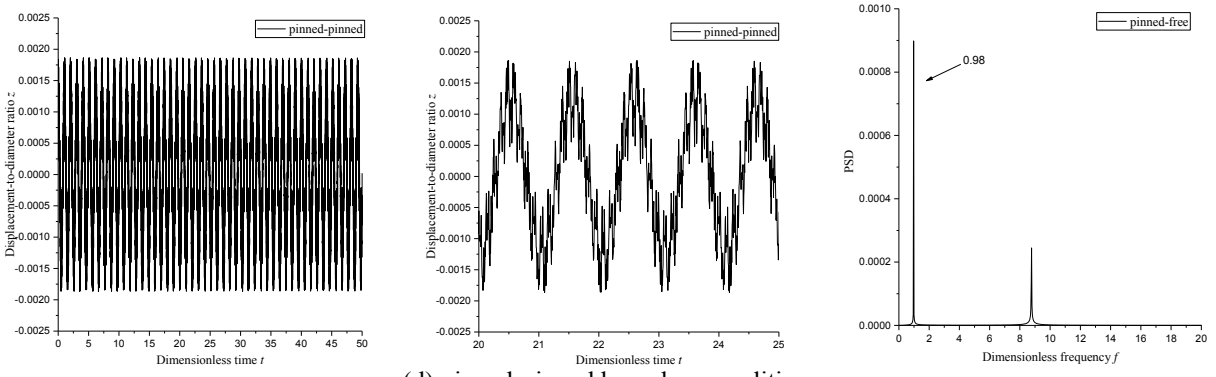

(d) pinned-pinned boundary condition

Figure 2: Free vibration time history and frequency analysis of the free span midpoint under different boundary conditions

The internal flow velocity ignored, the structural natural frequencies of the first three modes are calculated and presented in Table 3. For the free span under the fixed-fixed boundary condition, the vortex-shedding frequencies coincides with the first three structural natural frequencies when the external current velocities respectively are 1.42 m/s, 3.93 m/s, 7.70 m/s, according to Strouhal principle. In a similar manner, for the free span under the fixed-pinned boundary condition, the vortex-shedding frequencies coincides with the first three structural natural frequencies when the external current velocities respectively are 0.98 m/s, 3.18 m/s, 6.64 m/s. For the free span under the fixed-free boundary condition, the vortex-shedding frequencies coincides with the first three structural natural frequencies when the external current velocities respectively are 0.22 m/s, 1.40 m/s, 3.93 m/s. And for the free span under the pinned-pinned boundary condition, the vortex-shedding frequencies coincides with the first three structural natural frequencies when the external current velocities respectively are 0.63 m/s, 2.51 m/s, 5.65 m/s. Since the boundary conditions determines the natural frequency of the pipeline free span, the current velocity range that makes the lock-in occur varies when the boundary conditions changes. The results mentioned above are also summarised in Table 4.

Table 3 Fundamental natural frequency of the pipeline free span under different boundary conditions.

Boundary condition	1st mode natural frequency $f_{s,1}$ (Hz)	2nd mode natural frequency $f_{s,2}$ (Hz)	3rd mode natural frequency $f_{s,3}$ (Hz)
fixed-fixed	0.81	2.24	4.40
fixed-pinned	0.56	1.82	3.79
fixed-free	0.13	0.80	2.24
pinned-pinned	0.36	1.44	3.23

Table 4 Current velocity for vortex-shedding frequency equal to the structural natural frequency of the first three modes.

Boundary condition	Current velocity (m/s) $\Omega_f = f_{s,1}$	Current velocity (m/s) $\Omega_f = f_{s,2}$	Current velocity (m/s) $\Omega_f = f_{s,3}$
fixed-fixed	1.42	3.93	7.70
fixed-pinned	0.98	3.18	6.64
fixed-free	0.22	1.40	3.93
pinned-pinned	0.63	2.51	5.65

The mode shapes of the free span under four different boundary conditions at their corresponding three current velocities provided in Table 4 are shown in Figures 4-7. The boundary conditions determine the natural frequencies of the free-spanning pipeline system, thereby changing the lock-in region of the system. Results show that the lock-in happens at the lowest current velocity ranges with the fixed-free boundary condition, and at the highest current velocity ranges with the fixed-fixed boundary condition.

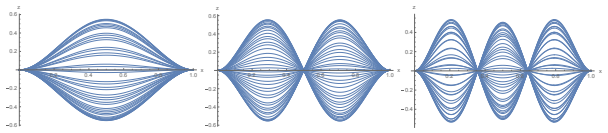

(a) 1.42 m/s (b) 3.93 m/s (c) 7.70 m/s

Figure 4: Mode shapes of the free span under the fixed-fixed boundary condition.

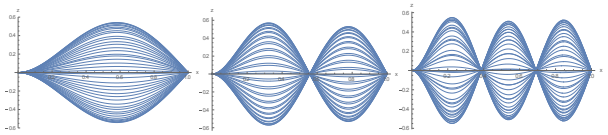

(a) 0.98 m/s (b) 3.18 m/s (c) 6.64 m/s

Figure 5: Mode shapes of the free span under the fixed-pinned boundary condition.

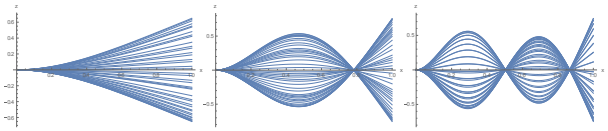

(a) 0.22 m/s (b) 1.40 m/s (c) 3.93 m/s

Figure 6: Mode shapes of the free span under the fixed-free boundary condition.

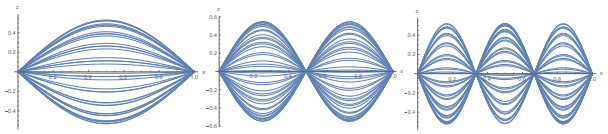

(a) 0.63 m/s (b) 2.51 m/s (c) 5.65 m/s

Figure 7: Mode shapes of the free span under the pinned-pinned boundary condition.

4.3 DYNAMIC ANALYSIS

Figure 8 presents how the reduced velocity *Vr* affects maximum RMS displacement-to-diameter ratio $z_{\text{RMS, Max}}$ of the free-spanning pipeline within the lock-in region. Results show that the lock-in occurs within the same reduced velocity region for the four boundary conditions discussed, i.e., $Vr \in [4, 8]$ and the tendency of $z_{\text{RMS, Max}}$ with the change of *Vr* is similar for the four boundary conditions. However, there is a distinct disparity for the value of $z_{\text{RMS, Max}}$ between different boundary conditions,

with the fixed-free pipeline having the minimum $z_{\mathrm{RMS,\,Max}}$, followed by the fixed-fixed, the fixed-pinned, and the pinned-pinned which has the maximum $z_{\mathrm{RMS,\,Max}}$.

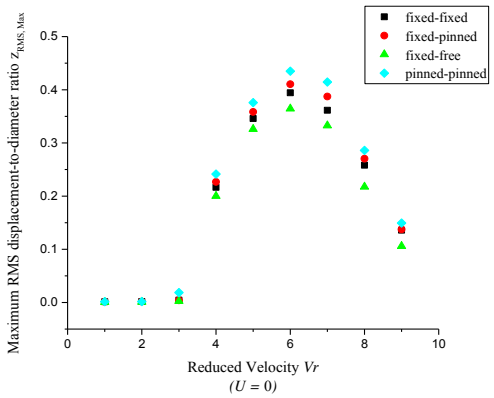

Figure 8: Effect of the reduced velocity on the maximum RMS displacement-to-diameter ratio.

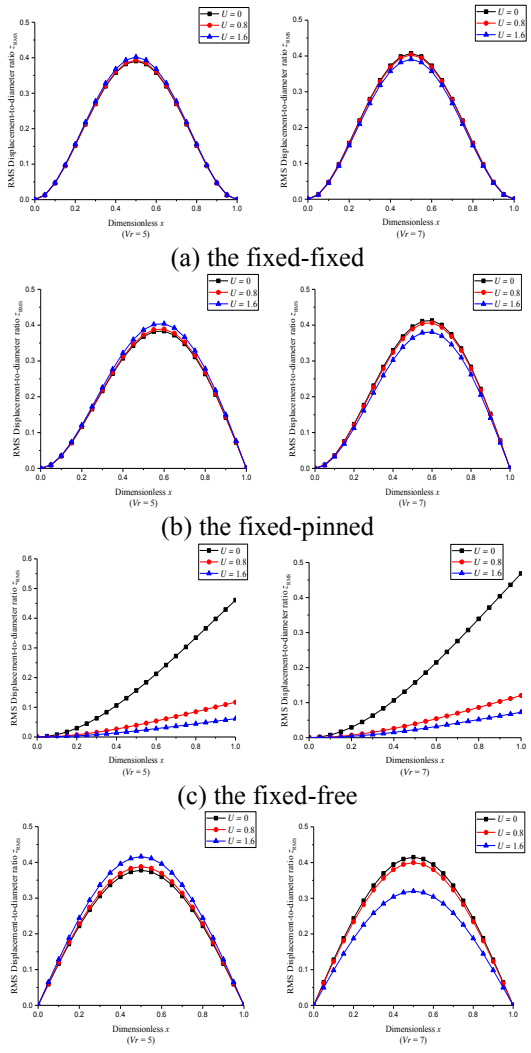

Figure 9: Distribution of RMS displacement-to-diameter ratio of the free-spanning pipeline.

Figure 9 demonstrates how the internal flow velocity U affects RMS displacement-to-diameter ratio z_{RMS} of the free-spanning pipeline under different boundary conditions. Results are calculated with Vr = 5, 7 and U = 0, 0.8, 1.6. Results show that the internal flow velocity will alter the z_{RMS} along the pipeline free span. When the internal flow velocity varies, there is a sharp change in the spanwise z_{RMS} for the free span with the fixed-free boundary condition. For the pinned-pinned free span, the change of the spanwise z_{RMS} is also remarkable.

Figure 10 exhibits the influence of internal flow velocity change on the natural frequency of the pipeline free span. For the free span with fixed-fixed, fixed-pinned or pinned-pinned boundary condition, the structural natural frequency declines with the increase of internal flow velocity. When the velocity of the internal flow surpasses a critical value, i.e. the dimensionless U = 7.56, 5.40, 3.78, respectively for the fixed-fixed, fixed-pinned or pinned-pinned ended free span, the pipeline system will lose its stability through first mode buckling due to the centrifugal force acting on the structure by the internal flow. However, the results in Figure 10 does not include the pipeline system with fixed-free boundary condition, since the vibration becomes non-conservative because the system can exchange energy with the environment as the free end discharges fluid (Meng, 2017).

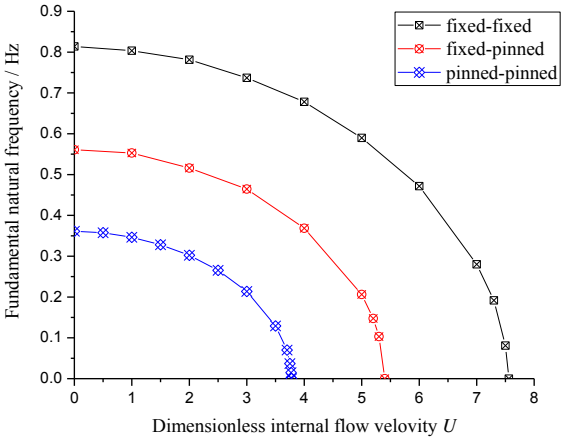

Figure 10: Effect of boundary conditions on the critical internal velocity

5. CONCLUSION

In the present paper, the eigenvalue problems for the cross-flow vibration of the free-spanning submarine pipeline conveying internal fluid are studied for four different boundary conditions, and the solution of natural frequency based on GITT is put forward and validated. Besides, the mode shapes and dynamic behaviours of the pipeline free span are discussed with different boundary conditions, and internal and external flow velocities are discussed. The methodology and results in this paper can

also expand to solving even more complicated boundary-value problems. Findings are summarised as follows.

- Based on GITT, the structural natural frequencies of the free-spanning submarine pipeline constrained by four different boundary conditions are calculated and verified against the theoretical results.
- Since the boundary conditions determines the natural frequency of the pipeline free span, the current velocity range that makes the lock-in occur varies when the boundary condition changes. Under the fixed-fixed boundary condition, the lock-in happens at the highest current velocity range.
- The lock-in region is $Vr \in [4, 8]$ for all the boundary conditions, since the reduced velocity Vr is calculated based on the structural natural frequency, which changes according to the boundary conditions. The tendency of $z_{\mathrm{RMS,\,Max}}$ with the change of Vr is similar for the four boundary conditions discussed in the present paper. However, there is a distinct disparity for the value of $z_{\mathrm{RMS,\,Max}}$ between different boundary conditions.
- The boundary condition influences the natural frequency of the free-spanning pipeline system, and also the critical internal flow velocity for structural instability.

6. ACKNOWLEDGEMENTS

This work is supported by National Key Research and Development Plan of China (Grant No. 2016YFC0303700), National Natural Science Foundation of China (Grant No. 51509258), National Science and Technology Major Project of China (2016ZX05033-004-004) and Science Foundation of China University of Petroleum, Beijing (No. 2462013YJRC003 and No. 2462015YQ0403).

7. REFERENCES

1. RONOLD, K. O. (1995) *A probabilistic approach to the lengths of free pipeline spans*. Appl. Ocean Res. 17(4): 225-232.
2. BOUCHONNEAU, N., SAUVANT-MOYNOT, V., CHOQUEUSE, D., GROSJEAN, F., PONCET, E., PERREUX, D. (2010) *Experimental testing and modeling of an industrial insulated pipeline for deep sea application*. J. Pet. Sci. Eng. 73(1-2): 1-12.
3. FYRILEIV, O., AAMLID, O., VENAS, A., COLLBERG, L. (2013) *Deepwater pipelines - status, challenges and future trends*. Proc. IMechE M.: J. Eng. Marit. Environ. 227(4): 3 81-95.
4. SOLLUND, H. A., VEDELD, K., FYRILEIV, O. (2015) *Modal response of free spanning pipelines based on dimensional analysis*. Appl. Ocean Res. 50: 13-29.
5. DNV-RP-F105 (2006) *Free Spanning Pipelines*. Norway: Det Norske Veritas.
6. LOU, M., DING, J., GUO, H. Y., DONG, X. L. (2005) *Effect of internal flow on vortex-induced vibration of submarine free spanning pipelines*. China Ocean Eng. 19: 147-154.
7. KAEWUNRUEN, S., CHIRAVATCHRADEJ, J., CHUCHEEPSAKUL, S. (2005) *Nonlinear free vibrations of marine risers/pipes transporting fluid*. Ocean Eng. 32(3-4): 417-440.
8. BRUSCHI, R., VITALI, L. (1991) *Large amplitude oscillations of geometrically non-linear elastic beams subjected to hydrodynamic excitation*. J. Offshore Mech. Arct. Eng. 113(2).
9. GU, J. J., VITOLA, M., COELHO, J., PINTO, W. T., DUAN, M. L., LEVI, C. (2013a) *An experimental investigation by towing tank on VIV of a long flexible cylinder for deepwater riser application*. J. Mar. Sci. Technol. 18: 358-369.
10. GU, J. J., PINTO, W. T., LEVI, C., DUAN, M. L. (2013b) *An experimental study of the spanwise correlation of vortex shedding in the towing tank*. Ships. Offshore Struc. 8(5): 517-523.
11. CHOI, H. S. (2001) *Free spanning analysis for offshore pipeline*. Ocean Eng. 28(2001): 1325-1338.
12. MENG, S., KAJIWARA, H., ZHANG, W. (2017) *Internal flow effect on the cross-flow vortex-induced vibration of a cantilevered pipe discharging fluid*. Ocean Eng. 137: 120-128.
13. CUI. H., TANI, J. (2008) *Effect of boundary conditions on the stability of a cantilever pipe discharging and aspirating fluid*. JSME Int. J. 39(1): 20-24.
14. AI, S. M., SUN, L. P., MA, G. (2009). *The effect of soil non-linearity on VIV response of a free spanning pipeline*. In: Proceedings of the 28th international conference on ocean, offshore and arctic engineering, OMAE2009-79063, Hawaii.
15. TANG, M., YANG, C., YAN, J., YUE, Q. (2015). *Validity and limitation of analytical models for the bending stress of a helical wire in unbonded flexible pipes*. Appl. Ocean Res. 50: 58-68.
16. YANG, Z., YAN, J., CHEN, J., LU, Q., YUE, Q. (2017). *Multi-Objective Shape Optimization Design for Liquefied Natural Gas Cryogenic Helical Corrugated Steel Pipe*. J. Offshore Mech. Arct. Eng. 139(5), 051703.
17. LI, T. T., LI, X.Z., LIANG, W., SU, J., AN, C., DUAN, M. L. (2016) *A semi-analytical solution of the dynamic behaviour of free-spanning submarine pipelines conveying fluid*. In: Proceedings of the 26th international offshore and polar engineering conference, Rhodes.
18. FACCHINETTI, M.L., DE LANGRE, E., BIOLLEY, F. (2004) *Coupling of structure and wake oscillators in vortex-induced vibrations*. J. Fluids Struct. 19(2): 123-140.